Available online at www.sciencedirect.com
ScienceDirect
Journal of Solid State Chemistry 181 (2008) 166–174
JOURNAL OF SOLID STATE CHEMISTRY
www.elsevier.com/locate/jssc

Selective solution-phase synthesis of BiOCl, $BiVO_4$ and δ-Bi_2O_3 nanocrystals in the reaction system of $BiCl_3$–NH_4VO_3–NaOH

Xiang Ying Chen[a,*], Zhong Jie Zhang[b], Soon W. Lee[c,**]

[a]*Department of Applied Chemistry, School of Chemical Engineering, Hefei University of Technology, Hefei, Anhui 230009, PR China*
[b]*Department of Chemical Engineering, College of Chemistry and Chemical Engineering, Anhui University, Hefei, Anhui 230039, PR China*
[c]*Department of Chemistry (BK21), Sungkyunkwan University, Natural Science Campus, Suwon 440-746, Republic of Korea*

Received 20 August 2007; received in revised form 20 October 2007; accepted 26 October 2007
Available online 6 November 2007

Abstract

In this study, we demonstrate a straightforward solution-phase method for the selective synthesis of BiOCl, $BiVO_4$ and δ-Bi_2O_3 nanocrystals by simply manipulating the reaction temperature and the $BiCl_3$-to-NaOH mole ratio in the reaction system of $BiCl_3$–NH_4VO_3–NaOH. The experimental results revealed that BiOCl, as the sole product, was prepared when designating the reaction temperature ranging from room temperature to 100 °C, regardless of the $BiCl_3$-to-NaOH mole ratio; on the other hand, BiOCl, $BiVO_4$, and δ-Bi_2O_3 nanocrystals could be selectively prepared at 140–180 °C, depending on the $BiCl_3$-to-NaOH mole ratio in solution. Significantly, we first report on fabricating δ-Bi_2O_3 sample, the high-temperature cubic phase commonly stabilized at 730–824 °C, at the low reaction temperature of 140–180 °C under solution-phase synthetic conditions. In addition, the δ-Bi_2O_3 sample exhibits strong emission at room temperature.

Keywords: Solution-phase; Bismuth compounds; Nanomaterials; Photoluminescence

1. Introduction

Miniaturization of materials and devices in the scope of nanoscale are recently the focus in many areas mainly owing to the novel properties in comparison to their counterpart, depending on the shape, size and crystallinity. On the other hand, environment protection is becoming an important but realistic issue in the process of industrial production and application, which stimulates us to explore and make use of the materials with low- or non-toxicity [1].

Currently, bismuth-containing compounds have attracted much attention due to their environmentally benign nature, excellent properties, and promising candidates in many application fields [2,3]. For example, BiOCl can serve as catalyst for the oxidative cracking of *n*-butane to lower alkenes [4], as well as photocatalyst [5]. $BiVO_4$ has three polymorphs of monoclinic phase (clinobisvanite), tetragonal phase (dreyerite), and orthorhombic phase (pucherite) and usually exhibits excellent photocatalytic properties [6–10]. Bi_2O_3 reveals diverse polymorphs including α-, β-, γ-, δ-, and ε-Bi_2O_3 with distinctive optical and electrical properties [2,11]. Especially, δ-Bi_2O_3 possesses the high-temperature cubic fluorite structure commonly stabilized at 730–824 °C. It is recognized as one of the utmost promising solid electrolyte in the fields of fuel cells, sensors, and membranes because of its high oxygen ionic conductivity [12,13]. To date, δ-Bi_2O_3 nanowires were obtained by thermal conversion of Bi nanowires at 350 or 750 °C [14,15]; δ-Bi_2O_3 thin films were prepared by reactive sputtering [16] or CVD method [17]. However, as much as we know, no systematical investigation on the controllable synthesis of BiOCl, $BiVO_4$ and δ-Bi_2O_3 nanocrystals in one reaction system has been performed via a simple solution-phase route.

Herein, we demonstrate a facile solution-phase method to selectively prepare BiOCl, $BiVO_4$ and δ-Bi_2O_3 samples in the reaction system of $BiCl_3$–NH_4VO_3–NaOH. It was found that the reaction temperature and the $BiCl_3$-to-NaOH mole

*Corresponding author. Fax: +86 551 2901450.
**Also corresponding author.
E-mail address: cxy@ustc.edu (X.Y. Chen).

0022-4596/$ - see front matter © 2007 Elsevier Inc. All rights reserved.
doi:10.1016/j.jssc.2007.10.031

ratio play the vital impacts on the synthesis of targeting samples. This is the first route to prepare high-temperature phase δ-Bi_2O_3 sample at relatively low reaction temperature of 140–180 °C under solution-phase synthetic conditions. Additionally, the as-prepared δ-Bi_2O_3 sample exhibits strong room temperature emission.

2. Experimental section

All chemicals were purchased and used as received without further purification. The experiments were carried out in a 100 ml Teflon-lined stainless steel autoclave by adjusting the reaction temperature (i.e., room temperature, 60, 100, 140, 160, and 180 °C) and the initial $BiCl_3$-to-NaOH mole ratio (i.e., no NaOH, 1:2; 1:4; 1:6; 1:8; 1:10; 1:12, 1:14; and 1:16) while keeping the initial $BiCl_3$-to-NH_4VO_3 mole ratio as 1:1.

2.1. Typical synthetic procedure for preparing δ-Bi_2O_3 sample in the $BiCl_3$-to-NaOH mole ratio of 1:16

First, NH_4VO_3 (2 mmol) was dissolved in hot distilled H_2O (60 ml, 80–90 °C) to form a transparent solution, which was then cooled to room temperature. $BiCl_3$ (2 mmol) was further added into the above solution under stirring. After being stirred for 20 min, aqueous solution (20 ml) of NaOH (32 mmol) was gradually poured, giving rise to buffy suspension. Finally, the above suspension was transferred into a 100 ml Teflon-lined stainless steel autoclave, which was then sealed and kept at 160 °C in an electrical oven. After 12 h, the resulting white-yellow product was filtered off, washed with distilled water and absolute ethanol for several times, and then dried under vacuum at 60 °C for 6 h.

2.2. Characterization

X-ray powder diffraction (XRPD) patterns were obtained on a Rigaku Max-2200 with Cu$K\alpha$ radiation. Transmission electron microscope (TEM) and high-resolution transmission electron microscope (HRTEM) images were performed with a JEOL 2100F unit operated at 200 kV. Photoluminescent (PL) analysis was conducted with an AB2 spectrophotometer (Amico Bowmann).

3. Results and discussion

As is known, XRPD technique is a kind of powerful tool to characterize the phase, purity and crystallinity of the samples. Fig. 1 shows the typical XRPD patterns of samples prepared at room temperature for 12 h in various $BiCl_3$-to-NaOH mole ratios while keeping mole ratio of $BiCl_3$ and NH_4VO_3 as 1:1. We can see in Fig. 1 that all the XRPD patterns are almost the same, in accordance with the reported values for tetragonal BiOCl (JCPDS 06-0249), regardless of the various $BiCl_3$-to-NaOH mole ratios in solution. However, based on the further observation on

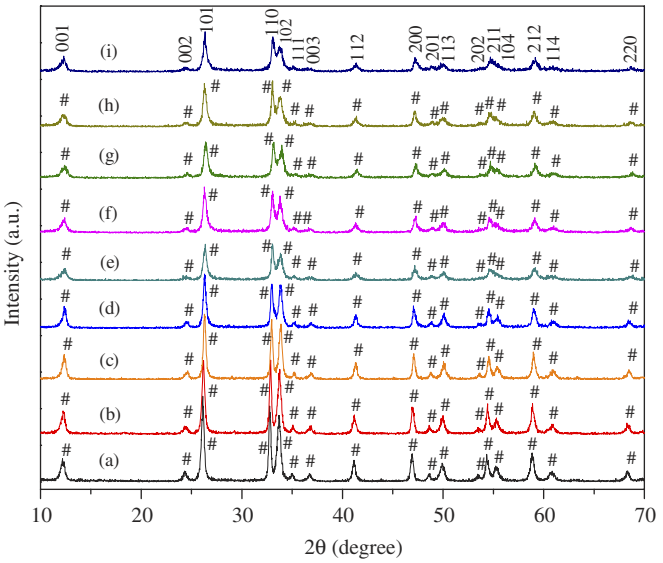

Fig. 1. XRPD patterns of samples prepared at room temperature for 12 h in various $BiCl_3$-to-NaOH mole ratios while keeping the $BiCl_3$-to-NH_4VO_3 mole ratio as 1:1: (a) no NaOH; (b) 1:2; (c) 1:4; (d) 1:6; (e) 1:8; (f) 1:10; (g) 1:12; (h) 1:14; and (i) 1:16. # tetragonal BiOCl (JCPDS 06-0249).

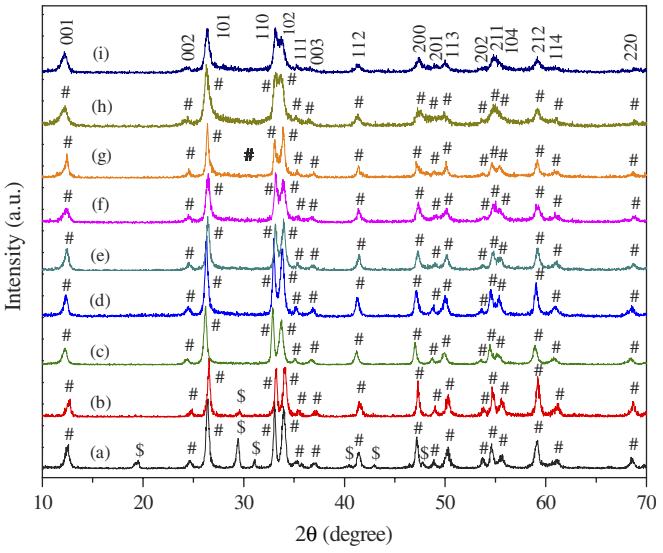

Fig. 2. XRPD patterns of samples prepared at 60 °C for 12 h in various $BiCl_3$-to-NaOH mole ratios while keeping the $BiCl_3$-to-NH_4VO_3 mole ratio as 1:1: (a) no NaOH; (b) 1:2; (c) 1:4; (d) 1:6; (e) 1:8; (f) 1:10; (g) 1:12; (h) 1:14; and (i) 1:16. # tetragonal BiOCl (JCPDS 06-0249) and $ monoclinic $BiVO_4$ (JCPDS 14-0688).

XRPD patterns in Fig. 1, we can find that the reflection peaks therein, e.g., (101), (110), and (102), gradually become broad with increasing the $BiCl_3$-to-NaOH mole ratio in solution. This phenomenon suggests that some of the characteristics (shape, size or crystallinity) of BiOCl samples might have somewhat shifted under the influence of the $BiCl_3$-to-NaOH mole ratio.

Fig. 2 depicts the typical XRPD patterns of samples prepared at 60 °C for 12 h in various $BiCl_3$-to-NaOH mole

ratios while keeping the $BiCl_3$-to-NH_4VO_3 mole ratio as 1:1. When in the absence of any amount of NaOH in solution, the resultant product consists of predominant tetragonal BiOCl (JCPDS 06-0249) and minor monoclinic $BiVO_4$ (JCPDS 14-0688), as shown in Fig. 2a. Meanwhile, in the case of $BiCl_3$-to-NaOH mole ratio as 1:2, the XRPD pattern in Fig. 2b indicates that the sample is mainly tetragonal BiOCl (JCPDS 06-0249) together with the trace monoclinic $BiVO_4$ (JCPDS 14-0688). When further increasing the $BiCl_3$-to-NaOH mole ratios from 1:4 to 1:16, the corresponding samples are all indexed as tetragonal BiOCl (JCPDS 06-0249), as shown in Figs. 2c–i. In addition, the reflection peaks of these XRPD patterns are growing broad as a function of the $BiCl_3$-to-NaOH mole ratio.

The typical XRPD patterns of samples prepared at 100 °C for 12 h in various $BiCl_3$-to-NaOH mole ratios while keeping the $BiCl_3$-to-NH_4VO_3 mole ratio as 1:1 are displayed in Fig. 3. In the absence of NaOH in solution, we can obtain the mixture of tetragonal BiOCl (JCPDS 06-0249) and monoclinic $BiVO_4$ (JCPDS 14-0688), as shown in Fig. 3a. When adjusting the $BiCl_3$-to-NaOH mole ratio to 1:2, the resulting sample consists of major monoclinic $BiVO_4$ and minor tetragonal BiOCl in Fig. 3b. Interestingly, when further increasing the $BiCl_3$-to-NaOH mole ratio to 1:4, the product is made up of sole tetragonal BiOCl without the obvious reflection peaks assignable to monoclinic $BiVO_4$. And the samples prepared in the $BiCl_3$-to-NaOH mole ratios of 1:6–1:16 are all identified as tetragonal BiOCl, similar to those obtained in Figs. 1 and 2.

Since the reaction temperature and $BiCl_3$-to-NaOH mole ratio have the important roles in the reaction system of $BiCl_3$–NH_4VO_3–NaOH, as elucidated in Figs. 1–3, we decided to further enhance the reaction temperature to 140 °C to find out the possible rules therein. Fig. 4 demonstrates the typical XRPD patterns of samples prepared at 140 °C for 12 h in various $BiCl_3$-to-NaOH mole ratios while keeping the $BiCl_3$-to-NH_4VO_3 mole ratio as 1:1. We can see in Fig. 4a that the mixture of tetragonal BiOCl (JCPDS 06-0249) and monoclinic $BiVO_4$ (JCPDS 14-0688) forms without introducing any amount of NaOH in solution. In the case of the $BiCl_3$-to-NaOH mole ratio of 1:2, monoclinic $BiVO_4$ appears to be predominant in the sample, as shown in Fig. 4b. Meanwhile, in the cases of the $BiCl_3$-to-NaOH mole ratios of 1:4–1:10, pure phase of tetragonal BiOCl occurs in Figs. 4c–f. It is noteworthy in Figs. 4g and h that some reflection peaks assignable to cubic δ-Bi_2O_3 (JCPDS 27-0052) appear and the high-temperature phase of cubic δ-Bi_2O_3 product ultimately forms as the sole target in the $BiCl_3$-to-NaOH mole ratio of 1:16, as shown in Fig. 4i.

Fig. 5 gives us the typical XRPD patterns of samples prepared at 160 °C for 12 h in various $BiCl_3$-to-NaOH mole ratios while keeping the $BiCl_3$-to-NH_4VO_3 mole ratio as 1:1. When in the absence of NaOH in solution, the sample contains major part of monoclinic $BiVO_4$ (JCPDS 14-0688) and minor part of tetragonal BiOCl (JCPDS 06-0249), as shown in Fig. 5a. With increasing the $BiCl_3$-to-NaOH mole ratio to 1:2, the resulting sample can be primarily identified as pure monoclinic $BiVO_4$ in Fig. 5b. However, when further increasing the $BiCl_3$-to-NaOH mole ratio to 1:8, 1:10 or 1:12, some other reflection peaks such as anorthic $Bi_{3.5}V_{1.2}O_{8.25}$ (JCPDS 52-1886) and cubic δ-Bi_2O_3 (JCPDS 27-0052) appear in Figs. 5e–g. Significantly, the pure cubic δ-Bi_2O_3 sample comes into being in the $BiCl_3$-to-NaOH mole ratio of 1:14 or 1:16, as revealed in Figs. 5h and i.

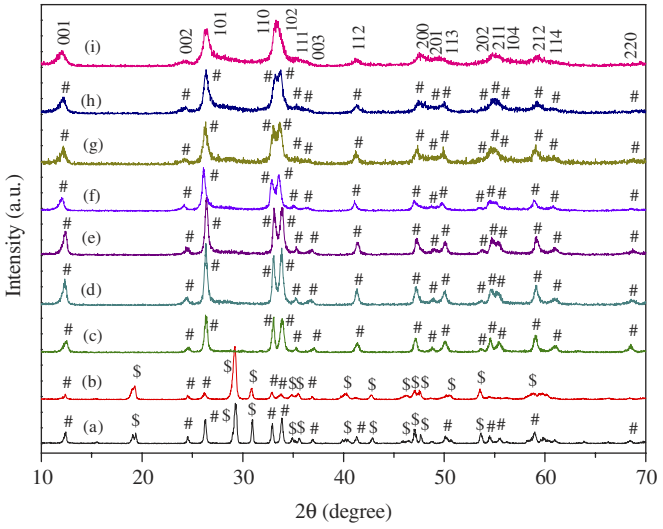

Fig. 3. XRPD patterns of samples prepared at 100 °C for 12 h in various $BiCl_3$-to-NaOH mole ratios while keeping the $BiCl_3$-to-NH_4VO_3 mole ratio as 1:1: (a) no NaOH; (b) 1:2; (c) 1:4; (d) 1:6; (e) 1:8; (f) 1:10; (g) 1:12; (h) 1:14; and (i) 1:16. # tetragonal BiOCl (JCPDS 06-0249) and $ monoclinic $BiVO_4$ (JCPDS 14-0688).

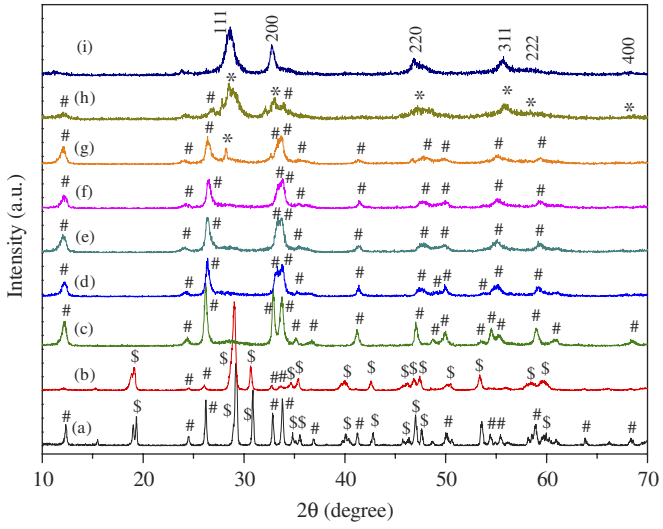

Fig. 4. XRPD patterns of samples prepared at 140 °C for 12 h in various $BiCl_3$-to-NaOH mole ratios while keeping the $BiCl_3$-to-NH_4VO_3 mole ratio as 1:1: (a) no NaOH; (b) 1:2; (c) 1:4; (d) 1:6; (e) 1:8; (f) 1:10; (g) 1:12; (h) 1:14; and (i) 1:16. # tetragonal BiOCl (JCPDS 06-0249), $ monoclinic $BiVO_4$ (JCPDS 14-0688) and * cubic δ-Bi_2O_3 (JCPDS 27-0052).

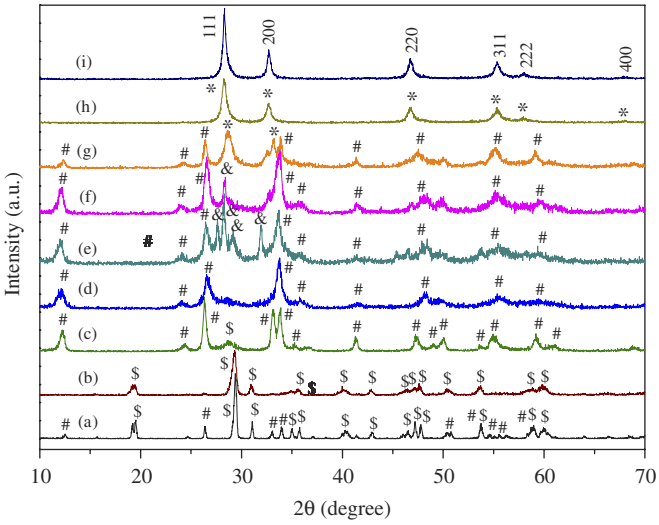

Fig. 5. XRPD patterns of samples prepared at 160 °C for 12 h in various $BiCl_3$-to-NaOH mole ratios while keeping the $BiCl_3$-to-NH_4VO_3 mole ratio as 1:1: (a) no NaOH; (b) 1:2; (c) 1:4; (d) 1:6; (e) 1:8; (f) 1:10; (g) 1:12; (h) 1:14; and (i) 1:16. # tetragonal BiOCl (JCPDS 06-0249), $ monoclinic $BiVO_4$ (JCPDS 14-0688), & anorthic $Bi_{3.5}V_{1.2}O_{8.25}$ (JCPDS 52-1886) and * cubic δ-Bi_2O_3 (JCPDS 27-0052).

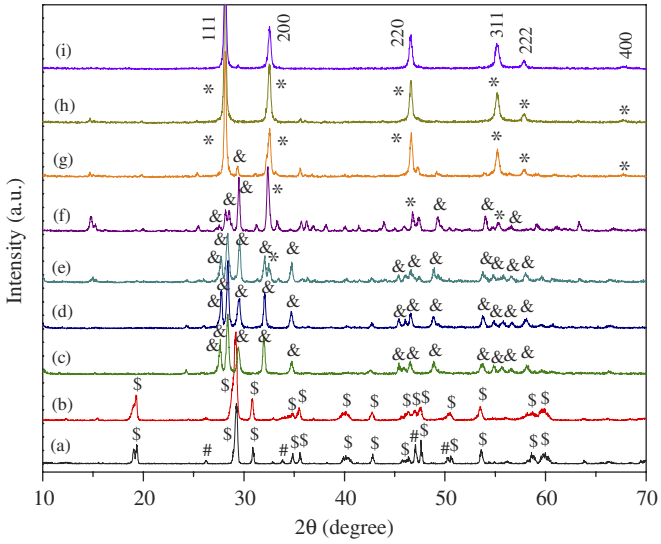

Fig. 6. XRPD patterns of samples prepared at 180 °C for 12 h in various $BiCl_3$-to-NaOH mole ratios while keeping the $BiCl_3$-to-NH_4VO_3 mole ratio as 1:1: (a) no NaOH; (b) 1:2; (c) 1:4; (d) 1:6; (e) 1:8; (f) 1:10; (g) 1:12; (h) 1:14; and (i) 1:16. # tetragonal BiOCl (JCPDS 06-0249), $ monoclinic $BiVO_4$ (JCPDS 14-0688), & anorthic $Bi_{3.5}V_{1.2}O_{8.25}$ (JCPDS 52-1886) and * cubic δ-Bi_2O_3 (JCPDS 27-0052).

The typical XRPD patterns of samples prepared at 180 °C for 12 h in various $BiCl_3$-to-NaOH mole ratios while keeping the $BiCl_3$-to-NH_4VO_3 mole ratio as 1:1 are indicated in Fig. 6. We can see in Fig. 6a that major monoclinic $BiVO_4$ (JCPDS 14-0688) together with minor tetragonal BiOCl (JCPDS 06-0249) engender in the absence of NaOH in solution. Analogous to that in Fig. 5b, we can obtain pure monoclinic $BiVO_4$ in the $BiCl_3$-to-NaOH mole ratio of 1:2, as shown in Fig. 6b. When further enhancing the $BiCl_3$-to-NaOH mole ratio to 1:4, 1:6, 1:8 or 1:10, the corresponding sample mainly consists of the unexpected anorthic $Bi_{3.5}V_{1.2}O_{8.25}$ (JCPDS 52-1886) in Figs. 6c–f. Furthermore, the pure cubic δ-Bi_2O_3 (JCPDS 27-0052) sample occurs in the $BiCl_3$-to-NaOH mole ratio of 1:14 or 1:16, as shown in Figs. 6h and i. However, compared with those in Figs. 5h and i, the reflection peaks in Figs. 6h and i are much thinner, which suggests that the sizes of δ-Bi_2O_3 crystals grow larger at 180 °C.

At the same time, TEM and HRTEM images were performed to vividly depict the shapes, sizes and intrinsic structures of the samples obtained in this study. Fig. 7a demonstrates the irregular flake-like nanostructures in high yielding of BiOCl sample prepared at room temperature for 12 h in the $BiCl_3$-to-NaOH mole ratio of 1:8 while keeping the $BiCl_3$-to-NH_4VO_3 mole ratio as 1:1. When increasing the $BiCl_3$-to-NaOH mole ratio to 1:16 at room temperature, the resultant sample consists of slightly aggregated nanoflakes, as shown in Fig. 7b. In regard to the BiOCl sample prepared at 60 °C for 12 h in the $BiCl_3$-to-NaOH mole ratio of 1:8 while keeping the $BiCl_3$-to-NH_4VO_3 mole ratio as 1:1, the corresponding TEM image illustrated in Fig. 7c reveals abundant irregular nanoflakes. When further increasing the $BiCl_3$-to-NaOH mole ratio to 1:16 at 60 °C, the typical TEM image in Fig. 7d indicates some congregated nanoflakes, similar to that in Fig. 7b. Concerning the BiOCl flake-like nanostructures in Figs. 7a–d, it is unambiguously correlated to its intrinsic layered structure by the combination of the chloride ion layer and the metal oxygen layer, as revealed in the inset of Fig. 7a. In order to clarify the substantial structure of these BiOCl nanoflakes, we conducted the HRTEM observation taken from Fig. 7d. To our surprise, these BiOCl nanoflakes are electron beam sensitive and break up into nanoparticles after being irradiated for tens of seconds, as described in Fig. 7e. An amplified individual nanoparticle (ca. 10 nm) in Fig. 7e is displayed in Fig. 7f, which has the typical lattice fringe of ca. 0.34 nm in accordance with that of (101) plane of BiOCl sample. In fact, novel syntheses of nanostructures under electron beam irradiation were previously reported, such as BN dendrites [18], Zn and ZnO nanobelts [19], carbon nanotubes [20], CdI_2 nanoparticles [21]. Hence, we believe that this kind of top-down strategy is an alternative way to fabricate BiOCl nanoparticles under the electron beam irradiation route, which might be extended to other kinds of irradiation sources such as γ-irradiation in the future.

Figs. 8a and b indicate the respective TEM image of BiOCl samples prepared at 100 °C for 12 h in the $BiCl_3$-to-NaOH mole ratio of 1:8 or 1:16 while keeping the $BiCl_3$-to-NH_4VO_3 mole ratio as 1:1, which result in flake-like nanostructures, similar to those in Figs. 7a–d. The HRTEM image of BiOCl nanoflakes in Fig. 8c also reveals the electron beam sensitive feature and the representative lattice spacing is ca. 0.34 nm, consistent with that of (101) plane of BiOCl sample. The SAED pattern taken from

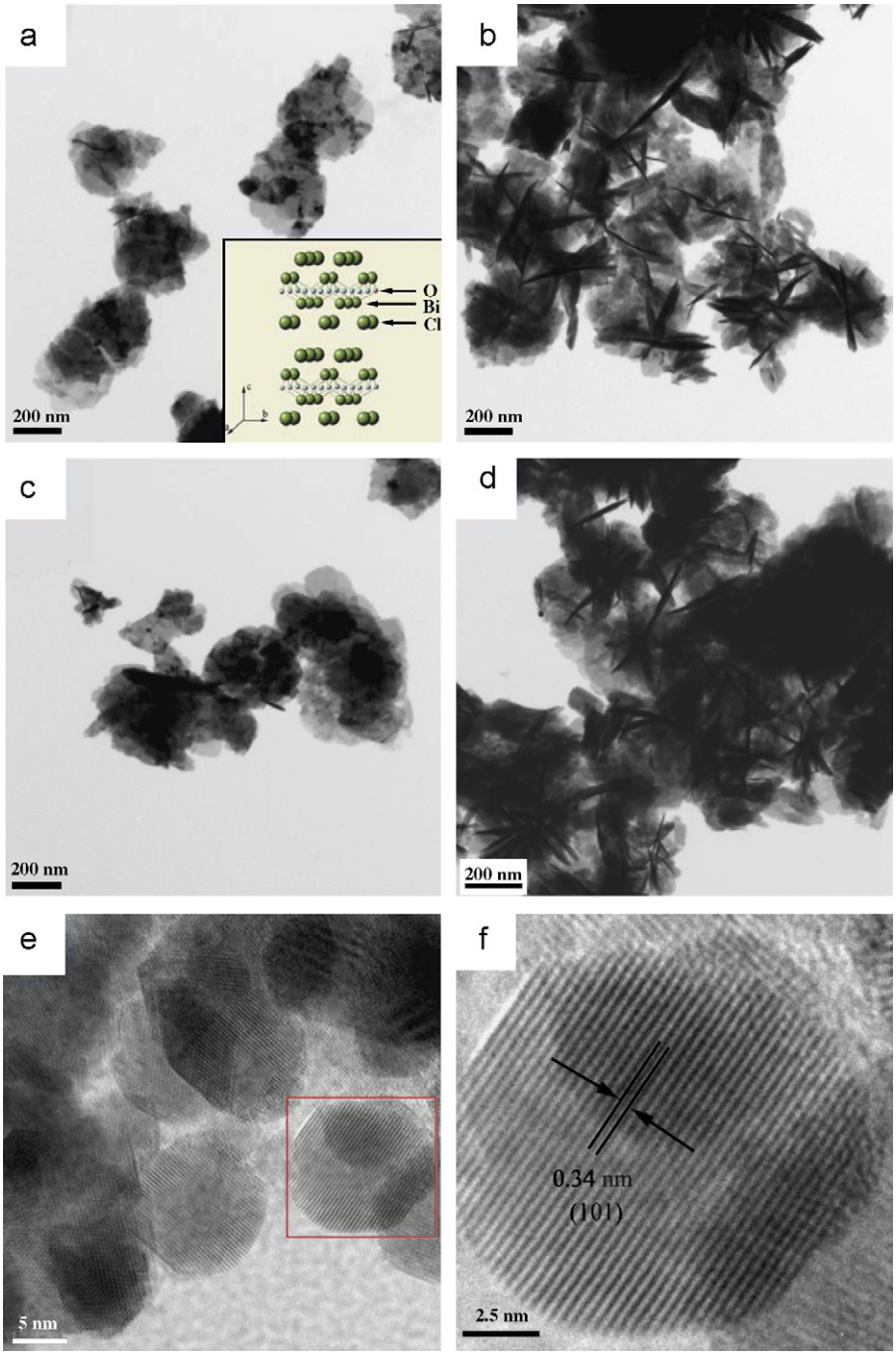

Fig. 7. (a) and (b) TEM images of BiOCl samples prepared at room temperature for 12 h in the respective $BiCl_3$-to-NaOH mole ratio of 1:8 and 1:16 while keeping the $BiCl_3$-to-NH_4VO_3 mole ratio as 1:1; (c) and (d) TEM images of BiOCl samples prepared at 60 °C for 12 h in the respective $BiCl_3$-to-NaOH mole ratio of 1:8 and 1:16 while keeping the $BiCl_3$-to-NH_4VO_3 mole ratio as 1:1; (e) and (f) HRTEM images taken from (d).

these BiOCl nanoflakes demonstrates the polycrystalline characteristics, as shown in Fig. 8d.

Figs. 9a and b display the TEM images of δ-Bi_2O_3 sample prepared at 160 °C for 12 h in the $BiCl_3$-to-NaOH mole ratio of 1:14 while keeping the $BiCl_3$-to-NH_4VO_3 mole ratio as 1:1, in which the sample is composed of small-sized nanoparticles. Similarly, we can see in Fig. 9c that the δ-Bi_2O_3 sample is made up of tiny nanoparticles prepared at 160 °C for 12 h in the $BiCl_3$-to-NaOH mole ratio of 1:16 while keeping the $BiCl_3$-to-NH_4VO_3 mole ratio as 1:1. Assisted with the HRTEM technique, these nanoparticles are ca. 10 nm and certain extent of aggregation occurs in Fig. 9d. Moreover, the lattice spacing of ca. 0.32 nm in Fig. 9e corresponds to that of (111) plane of δ-Bi_2O_3 sample. The corresponding SAED pattern in Fig. 9f reveals the polycrystalline feature of these nanoparticles and is identical with the results of XRPD patterns in Figs. 5h and i.

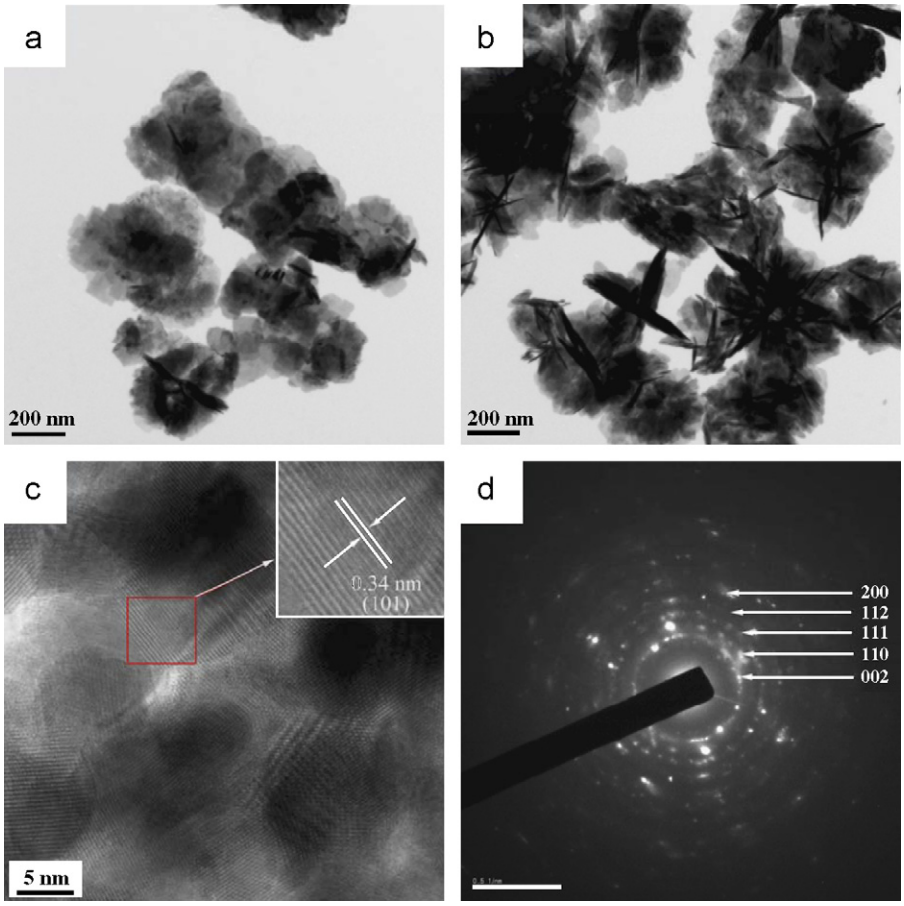

Fig. 8. TEM images of BiOCl samples prepared at 100 °C for 12 h in various $BiCl_3$-to-NaOH mole ratios while keeping the $BiCl_3$-to-NH_4VO_3 mole ratio as 1:1: (a) 1:8; and (b)–(d) 1:16.

As mentioned above, we prepared monoclinic $BiVO_4$ (clinobisvanite) sample at 180 °C for 12 h in the $BiCl_3$-to-NaOH mole ratio of 1:2 while keeping the $BiCl_3$-to-NH_4VO_3 mole ratio as 1:1 and the resulting TEM images are presented in Fig. 10. In terms of the TEM image with low magnification in Fig. 10a, the $BiVO_4$ sample comprises of dendritic nanostructures, approximate to the results obtained in the absence of any surfactant [8]. Further observation on these dendrites, we can find that a large number of nanoparticles adhere to the surfaces, as shown in Fig. 10b. The representative HRTEM image in Fig. 10c reveals the lattice spacing of ca. 0.29 nm, corresponding to that of (040) plane of $BiVO_4$ sample. On the other hand, the SAED pattern in Fig. 10d indicates the single-crystal feature with the typical crystal zone axis of [001].

On the basis of XRPD patterns and TEM images illustrated in Figs. 1–10, we can conclude that the reaction temperature and the $BiCl_3$-to-NaOH mole ratio (i.e., acidity) have the crucial roles in the selective formation of BiOCl, $BiVO_4$ and δ-Bi_2O_3 nanocrystals in the reaction system of $BiCl_3$–NH_4VO_3–NaOH. BiOCl sample forms immediately by the hydrolysis of $BiCl_3$ in aqueous solution [22], and no $BiVO_4$ or δ-Bi_2O_3 sample occurs at room temperature because of the deficient driving force to convert BiOCl into $BiVO_4$ or δ-Bi_2O_3 (in Fig. 1). When increasing the reaction temperature to 60 or 100 °C, the $BiVO_4$ together with BiOCl appears in the low $BiCl_3$-to-NaOH mole ratios and it seems that high $BiCl_3$-to-NaOH mole ratio is not in favor of the formation of $BiVO_4$, as shown in Figs. 2 and 3. Meanwhile, BiOCl, $BiVO_4$, and δ-Bi_2O_3 nanocrystals come forth by simply adjusting the $BiCl_3$-to-NaOH mole ratio in solution (in Figs. 4–6). It suggests that high reaction temperature and high acidity are indispensable for δ-Bi_2O_3 sample, while high reaction temperature and low acidity are for $BiVO_4$ sample. On the other hand, we recently prepared a series of bismuth oxo nanocrystals (BiOCl, $Bi_{12}O_{17}Cl_2$, α-Bi_2O_3, $(BiO)_2CO_3$), using $BiCl_3$ and NaOH as the starting materials without introducing NH_4VO_3 in solution [22]. It is notable that there exist two distinctive aspects between them. First, the present BiOCl sample is electron beam sensitive while the previous one is much stable. This is probably caused by the excessive dose of NaOH herein, which impacts the eroding effect on the BiOCl sample in solution. Secondly, the present outcome is the high-temperature phase of δ-Bi_2O_3 while the previous one is α-Bi_2O_3, probably due to the presence of vanadate ions in solution. It has been proved that β-Bi_2O_3 (the metastable phase) can be stabilized at lower temperature by the addition of certain amount of oxides or fluorides, such as CeO_2 [23], HfO_2

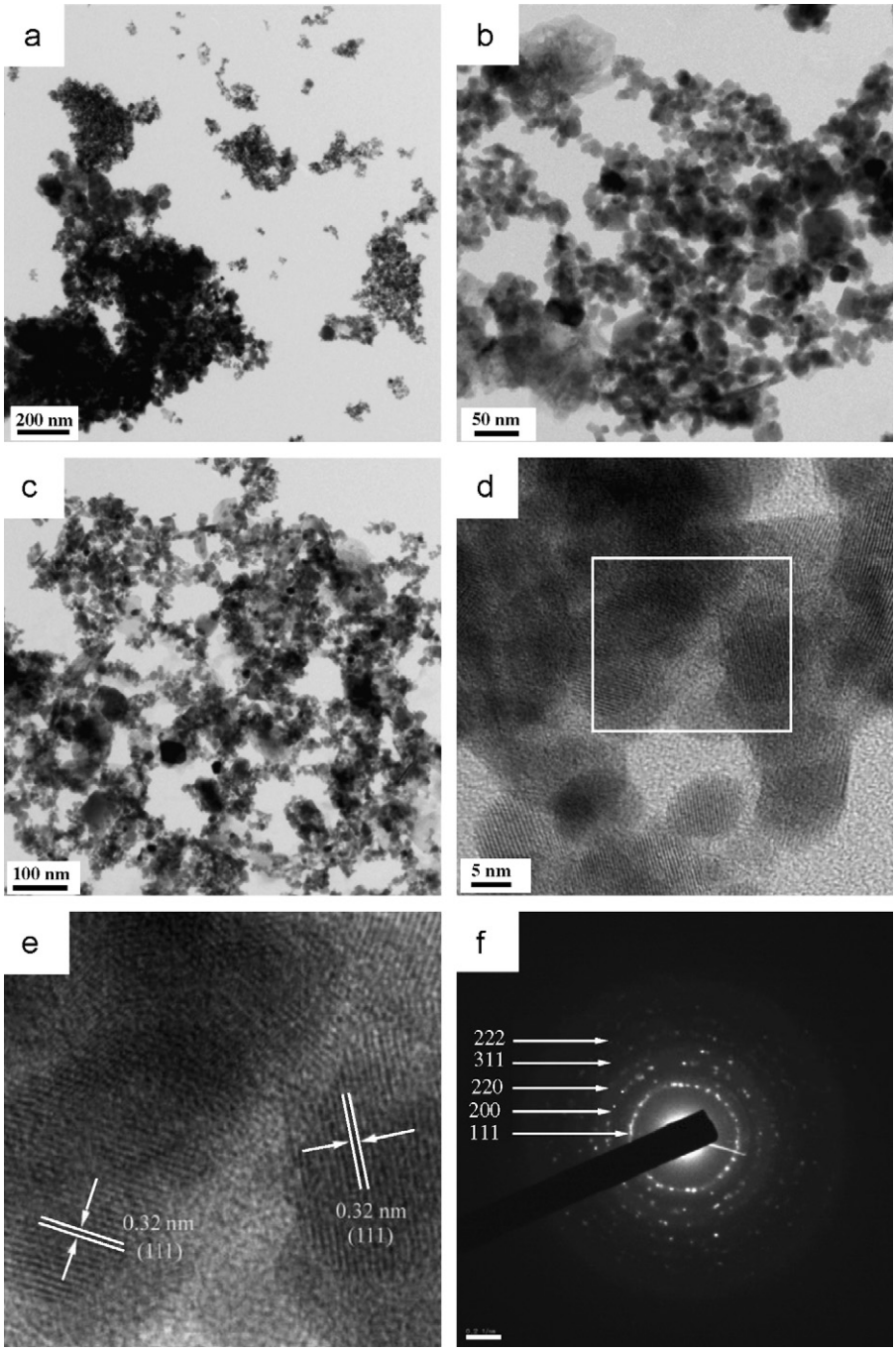

Fig. 9. TEM images of δ-Bi_2O_3 samples prepared at 160 °C for 12 h in various $BiCl_3$-to-NaOH mole ratios while keeping the $BiCl_3$-to-NH_4VO_3 mole ratio as 1:1: (a and b) 1:14 and (c)–(f) 1:16.

[24], and PbF_2 [25]. In order to determine the role of vanadates ions, we also conducted some parallel experiments by introducing other anions such as molybdates, tungstates in the absence of vanadates in solution. As a consequence, we can just obtain α-Bi_2O_3 instead of δ-Bi_2O_3, which indicates that the vanadates remaining in solution are indispensable for fabricating δ-Bi_2O_3 sample under present conditions.

As reported earlier, the band gaps (E_g) for α-, β-, and γ-Bi_2O_3 bulk materials are 2.85, 2.58, and 2.8 eV, respectively [26,27]. To our knowledge, there is no exact band gap value for δ-Bi_2O_3 bulk material reported so far although that for δ-Bi_2O_3 thin film was given as 1.3–1.9, 2.4–2.9 [15], or 3.0 eV [28], depending on various synthetic conditions. The present δ-Bi_2O_3 nanoparticles are expected to exhibit unique PL property probably owing to the quantum confinement effect. Fig. 11 shows the room temperature PL spectrum at $\lambda_{ex} = 220$ nm of δ-Bi_2O_3 nanoparticles prepared at 160 °C for 12 h in the $BiCl_3$-to-NaOH mole ratio of 1:16 while keeping the $BiCl_3$-to-NH_4VO_3 mole

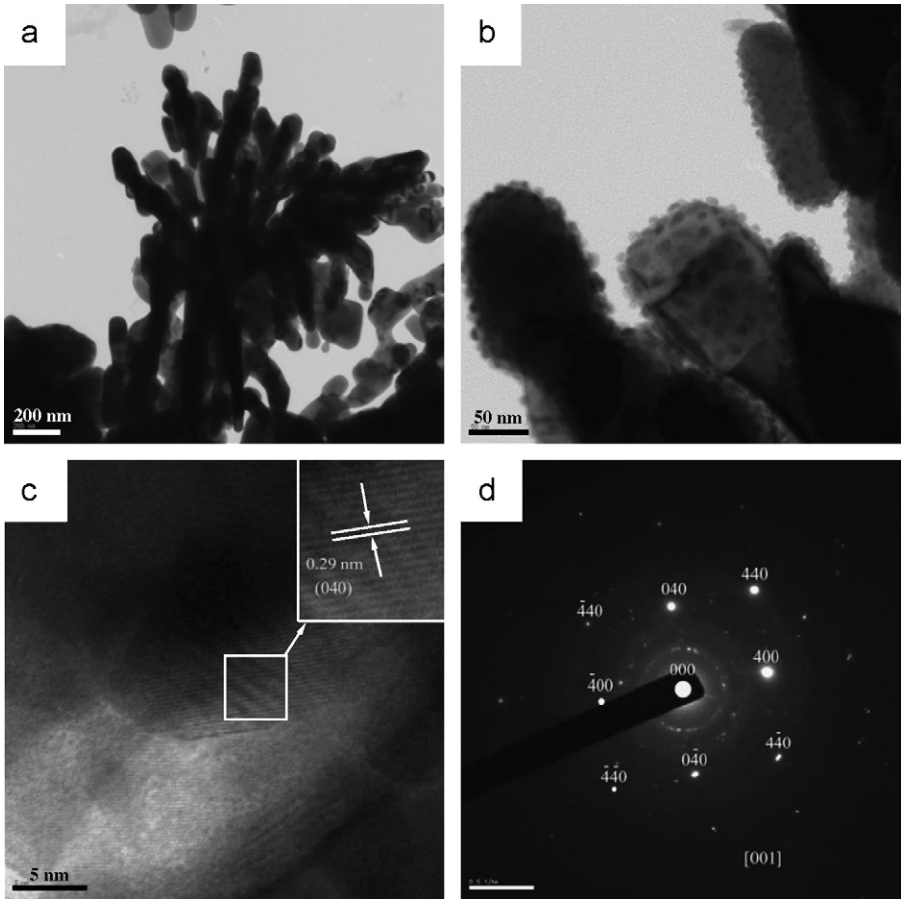

Fig. 10. TEM images of $BiVO_4$ sample prepared at 180 °C for 12 h in the $BiCl_3$-to-NaOH mole ratio of 1:2 while keeping the $BiCl_3$-to-NH_4VO_3 mole ratio as 1:1.

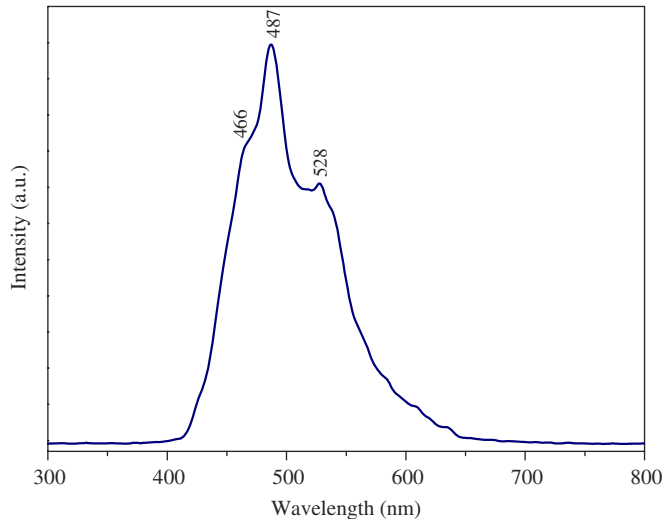

Fig. 11. Room temperature PL spectrum at $\lambda_{ex} = 220$ nm of δ-Bi_2O_3 nanoparticles prepared at 160 °C for 12 h in the $BiCl_3$-to-NaOH mole ratio of 1:16 while keeping the $BiCl_3$-to-NH_4VO_3 mole ratio as 1:1.

ratio as 1:1. The curve demonstrates several emission bands: one sharp and strong band at 487 nm (2.55 eV) as well as two weak shoulders at 466 nm (2.66 eV) and 528 nm (2.35 eV). On the other hand, Watson and co-workers reported that the high-temperature phase of δ-Bi_2O_3 adopts a defective fluorite structure with two oxygen vacancies per unit cell [29]. We thus presume that the PL property in Fig. 11 probably results from these oxygen vacancies. Further research on the PL result is undergoing.

4. Conclusion

In summary, BiOCl, $BiVO_4$ and δ-Bi_2O_3 nanocrystals were selectively prepared in the reaction system of $BiCl_3$–NH_4VO_3–NaOH through a facile solution-phase route. Some crucial growth parameters including the reaction temperature and the $BiCl_3$-to-NaOH mole ratio were systematically studied by means of XRPD and TEM techniques. It is of significance that the high-temperature phase of δ-Bi_2O_3 sample was first prepared at 140–180 °C in solution, which also exhibits strong emission at room temperature. The possible reaction mechanisms involved herein were discussed in brief. This kind of multi-component reaction system is expected to prepare other nanostructures with novel characteristics under mild conditions.

Acknowledgments

Financial support from Hefei University of Technology is gratefully appreciated. This work was also supported by the Korea Research Foundation Grant funded by the Korean Government (MOEHRD) (KRF-2005-005-J11902).

References

[1] X. Wang, J. Zhuang, Q. Peng, Y.D. Li, Nature 437 (2005) 121.
[2] M. Mehring, Coord. Chem. Rev. 251 (2007) 974.
[3] P.J. Sadler, H.Y. Li, H.Z. Sun, Coord. Chem. Rev. 185–186 (2007) 689.
[4] N. Kijima, K. Matano, M. Saito, T. Oikawa, T. Konishi, H. Yasuda, T. Sato, Y. Yoshimura, Appl. Catal. A 206 (2001) 237.
[5] K.L. Zhang, C.M. Liu, F.Q. Huang, C. Zheng, W.D. Wang, Appl. Catal. B 68 (2006) 125.
[6] A. Kudo, K. Omori, H. Kato, J. Am. Chem. Soc. 121 (1999) 11459.
[7] L. Zhou, W.Z. Wang, S.W. Liu, L.S. Zhang, H.L. Xu, W. Zhu, J. Mol. Catal. A 252 (2006) 120.
[8] L. Zhang, D.R. Chen, X.L. Jiao, J. Phys. Chem. B 110 (2006) 2668.
[9] S. Tokunaga, H. Kato, A. Kudo, Chem. Mater. 13 (2001) 4624.
[10] J.Q. Yu, A. Kudo, Adv. Funct. Mater. 16 (2006) 2163.
[11] B.J. Yang, M.S. Mo, H.M. Hu, C. Li, X.G. Yang, Q.W. Li, Y.T. Qian, Eur. J. Inorg. Chem. (2004) 1785.
[12] N.I. Medvedeva, V.P. Zhukov, V.A. Gubanov, D.L. Novikov, B.M. Klein, J. Phys. Chem. Solids 57 (1996) 1243.
[13] P. Shuk, H.D. Wiemhöfer, U. Guth, W. Göpel, M. Greenblatt, Solid State Ion. 89 (1996) 179.
[14] C.C. Huang, I.C. Leu, K.Z. Fung, Electrochem. Solid State Lett. 8 (2005) A204.
[15] L. Li, Y.W. Yang, G.H. Li, L.D. Zhang, Small 2 (2006) 548.
[16] H.T. Fan, S.S. Pan, X.M. Teng, C. Ye, G.H. Li, L.D. Zhang, Thin Solid Films 513 (2006) 142.
[17] T. Takeyama, Y. Kajikawa, N. Takahashi, T. Nakamura, S. Itoh, Chem. Vap. Depos. 12 (2006) 203.
[18] L.W. Yin, M.S. Li, Y.X. Liu, B. Xu, J.L. Sui, Y.X. Qi, Adv. Mater. 15 (2003) 720.
[19] Y.F. Yan, P. Liu, J.G. Wen, B. To, M.M. Al-Jassim, J. Phys. Chem. B 107 (2003) 9701.
[20] A. Yasuda, N. Kawase, W. Mizutani, J. Phys. Chem. B 106 (2002) 13294.
[21] R. Popovitz-Biro, N. Sallacan, R. Tenne, J. Mater. Chem. 13 (2003) 1631.
[22] X.Y. Chen, H.S. Huh, S.W. Lee, J. Solid State Chem. 180 (2007) 2510.
[23] X.L. Chen, W. Eysel, J. Solid State Chem. 127 (1996) 128.
[24] A. Ayala, A. López-Garcia, Solid State Commun. 99 (1996) 451.
[25] S. Horiuchi, F. Izumi, T. Mitsuhashi, K. Uchida, T. Shimomura, K. Ogasahara, J. Solid State Chem. 74 (1988) 247.
[26] Y.F. Qiu, D.F. Liu, J.H. Yang, S.H. Yang, Adv. Mater. 18 (2006) 2604.
[27] K. Gurunathan, Int. J. Hydrogen Energy 29 (2004) 933.
[28] A.A. Agasiev, A. Kh. Zeinally, S.J. Alekperov, Ya.Yu. Guseinov, Mater. Res. Bull. 21 (1986) 765.
[29] A. Walsh, et al., Phys. Rev. B 73 (2006) 235104.